Computation of rotating blade noise scattered by a centrifugal volute

Y Mao and **D Qi***
School of Energy and Power Engineering, Xi'an Jiaotong University, Xi'an, People's Republic of China

The manuscript was received on 8 April 2009 and was accepted after revision for publication on 29 May 2009.

DOI: 10.1243/09576509JPE794

Abstract: Noise radiating from rotating blades surrounded by a centrifugal volute is calculated combining a hybrid computational aeroacoustic method with the thin-body boundary element method (BEM), which considers the scattering effect of the volute to noise propagation. First, unsteady viscous flow in the centrifugal fan is simulated to obtain the noise sources information on the blades, and then the radiated noise in free field is computed using the Ffowcs Williams and Hawkings equation in the frequency domain. Lastly, the thin-body BEM is adopted to predict scattering effect of the volute. Good agreement between the numerical result and the exact solution of the plane wave scattered by a rigid flat plate validates the developed computational code. And the numerical result for blades noise shows that the scattering of the volute not only changes the directivity pattern of blades noise but also enhances the sound pressure level at the outlet of the volute.

Keywords: noise, scattering, centrifugal fan, blade, boundary element method

1 INTRODUCTION

Rotating blade is an essential component for many fluid machines, such as fans, pumps, compressors, and so on. Usually it not only transfers energy from drivers to the fluid, but also generates the aerodynamic noise.

The hybrid approach is the most widely used method to predict the aerodynamic noise of blades. In this approach, the unsteady flow is simulated to obtain the noise source information, and then the acoustic analogy or theory of vortex sound is used to predict the aerodynamic noise. Many investigators have used this approach to compute the noise of blades of fans. For example Lu *et al.* [**1**] and Maaloum *et al.* [**2**] numerically predicted the noise radiated from axial fan blades. Cho and Moon [**3**] and Moon *et al.* [**4**] calculated the aerodynamic noise generated from cross-flow fan blades using the Ffowcs Williams and Hawkings (FW–H) equation. As concerns centrifugal fans, many research groups have studied the tonal noise of impeller blades, such as Suaráz *et al.* [**5**, **6**], Qi *et al.* [**7**, **8**], Bakir *et al.* [**9**, **10**], and so on. All the above works have contributed to a deeper understanding of the aerodynamic noise generation mechanism of centrifugal fans. Also, all of them computed the blades noise using the Green function in free space, which implied that the scattering effect of the volute to noise propagation was neglected.

However, as the centrifugal fan is usually surrounded by a volute, the noise of blades does not radiate in free space, but scatters and diffracts on the wall of volute and impeller blades, as shown in Fig. 1. Early in the last century, experimental result of Moreland [**11**] has shown that the sound power spectrum was enhanced at various frequencies owing to the acoustic resonance in the volute. But to the best of authors' knowledge, few researchers have numerically studied the scattering effect of the volute to noise generated from the centrifugal blades, except Langthjem and Olhoff [**12**], who predicted the aerodynamic noise generated from a two-dimensional (2D) centrifugal pump impeller using the conventional boundary element method (BEM). The conventional BEM is usually used to analyse the sound radiation and scattering problem, but it requires the structure to be closed or to be a thick body, and if it is used to predict the noise of thin-body structure, such as volute,

**Corresponding author: School of Energy and Power Engineering, Xi'an Jiaotong University, 28 Xian Ning West Road, Xi'an, Shaanxi Province, 710049, People's Republic of China.*
email: dtqi@mail.xjtu.edu.cn; xjtupower@gmail.com

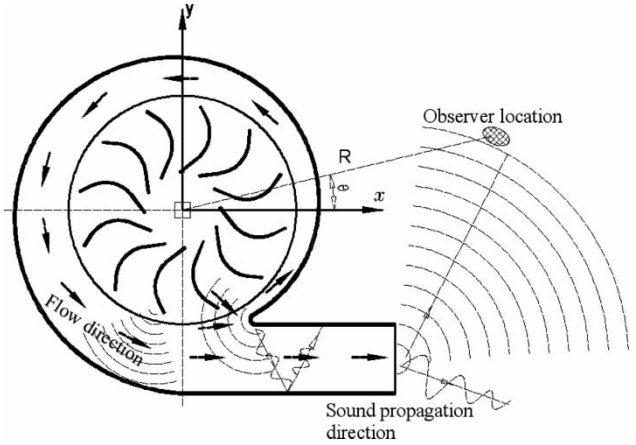

Fig. 1 Schematic of gas flow and sound radiation in the centrifugal fan

a thin-shape breakdown will occur [**13**]. In order to apply the conventional BEM to predict the centrifugal fan noise, Langthjem and Olhoff [**12**] constructed an imaginary surface at the outlet of volute to form a closed surface. But the flaws of this method are that the imaginary surface should be discretized and its acoustic impendence should be predefined with an artificial error. A thin-body BEM proposed by Wu and Wan [**14**], in which the discretization of the imaginary surface is not needed, has been applied to analyse the muffler performance [**15**] and sound propagation over a thin barrier [**16**]. Cho and Lee [**17**] used this method to calculate the sound radiation from a rotating dipole source in an opened thin duct, which could be regarded as an essential axial-flow fan model. Mao *et al.* [**18**] predicted the noise radiated from the volute of centrifugal fan using this method.

In this article, the thin-body BEM is applied to compute the noise radiated from the rotating blades, which focus on the scattering effect of the volute to noise propagation. For simplicity, a 2D model is used to calculate the unsteady flow and aerodynamic noise of the centrifugal fan, because the 2D aerodynamic design approach is usually applied to design the impeller blades and volute of centrifugal fans and pumps [**19**, **20**]. Clearly, the 2D model requires much less computational cost than that required by the three-dimensional (3D) model because of the reduction of computational domain, but all the actual flow and sound phenomena are 3D, and the 2D model could not capture all the flow and sound features. However, in the design process of centrifugal fans, the 2D model is useful and could find the trends, so we execute the numerical implementation using the 2D model all the same. And, of course, the 3D model could be developed using the similar method, and will be discussed in further work.

In what follows, section 2 introduces the simulation of the unsteady flow in the centrifugal fan in order to obtain the noise source information. The acoustic prediction is carried out in section 3, and section 4 gives some results and discussion. Conclusions are drawn in section 5.

2 UNSTEADY FLOW SIMULATION

2.1 Numerical model

The numerical simulation is made on an industrial centrifugal fan with 12 forward-curved blades rotating at 1450 r/min. 2D incompressible unsteady Navier–Stokes equations are solved using Fluent. Turbulence is simulated with the standard k–ε model. The discretization scheme of the time-dependent term is second of order, implicit. The pressure–velocity coupling is calculated using the SIMPLE algorithm. A second order, bounded central differencing scheme is used for convection and diffusion terms. The multi-domain structured meshes are generated to define the flow in the 2D model, as shown in Fig. 2. Slip mesh technique is used to transform the physical information at the interface between the blades outlet and the volute.

Time step length of the unsteady flow calculation has been set to $\Delta t = 1.1494 \times 10^{-4}$ s in order to obtain enough temporal resolution for the dynamic analysis, which corresponds to the time steps $T = 360$ during one impeller revolution. The number of iterations is adjusted to reduce the residual below an acceptable value in each time step. In particular, the ratio between the sum of the residuals and the sum of the fluxes for a given variable in all the cells is reduced to the value of 10^{-5}. More detailed introductions on the centrifugal fan and flow simulation are described in reference [**18**]. The same numerical procedure to compute the noise source has been adopted and validated by many previous researchers, such as Tajadura *et al.* [**6**], Younsi *et al.* [**9**], Khelladi *et al.* [**10**], and so on.

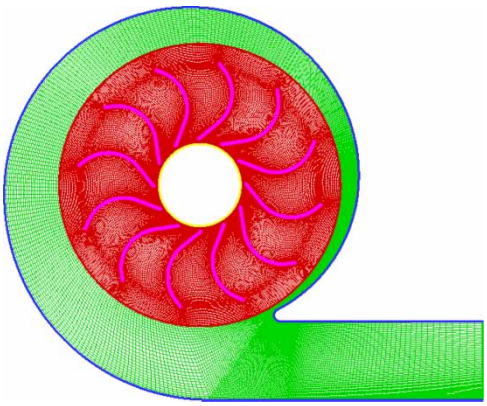

Fig. 2 Meshes of the 2D CFD model

2.2 Computation of blades position and pressure

In order to save the computational cost, only the original position $\boldsymbol{Y}_0$ and unit normal vector (UNV) $\boldsymbol{N}_0$ of the first blade are recorded in the simulation, and the position $\boldsymbol{Y}(m,t)$ and UMV $\boldsymbol{N}(m,t)$ of the mth blade at the tth time step are deduced as follows

$$\boldsymbol{Y}(m,t) = \boldsymbol{Y}_0 \exp\left[\frac{2\pi(m-1)\mathrm{i}}{Z}\right] \exp\left[\frac{2\pi(t-1)\mathrm{i}}{T}\right] \tag{1}$$

$$\boldsymbol{N}(m,t) = \boldsymbol{N}_0 \exp\left[\frac{2\pi(m-1)\mathrm{i}}{Z}\right] \exp\left[\frac{2\pi(t-1)\mathrm{i}}{T}\right] \tag{2}$$

where Z is the blades number, $m = 1, 2, \ldots, Z$, and $t = 1, 2, \ldots, T$. Similarly, only the static pressure P_0 on the first blade surface for one impeller revolution is recorded. The static pressure on the mth blade at the tth time step $P(m,t)$ is

$$P(m,t) = P_0\left\{\mathrm{mod}\left[t + \frac{(m-1)T}{Z}, T\right]\right\} \tag{3}$$

It should be noted that if the $\mathrm{mod}\{t + [(m-1)T/Z], T\}$ is equal to zero, $P(m,t)$ should be $P_0(T)$. The equations (1) to (3) are valid based on the following assumptions.

1. The blades are distributed circumferentially with even cascade spacing.
2. The pressure fluctuation on the blades is periodic, and the pressure values on different blades are nearly the same at a specific radial distance, when the circumferential angles of the blades are the same.

3 AERODYNAMIC NOISE PREDICTION

3.1 Free field of blades noise

The FW–H equation [**21**] is usually used to predict the noise generated by turbulent in the presence of arbitrarily moving bodies. The solution to the FW–H equation requires two surfaces and a volume integral. But for the low Mach flow, such as flow in the centrifugal fan, the noise is usually predominated by the dipole source [**22**, **23**]. In this article, we just consider the noise generated from the unsteady aerodynamic force on the blades.

The Dirac function in 3D Green function leads to a retarded time expression removing the temporal integration, while the Heaviside function in 2D Green function can only change the upper limit of the temporal integration to a finite value; the lower limit remains infinite. For 2D problems, it is more convenient to resolve the FW–H equation in the frequency domain [**24**, **25**]. The sound pressure $\Phi_\mathrm{I}(\boldsymbol{x},\omega)$ and its normal derivative $\partial\Phi_\mathrm{I}(\boldsymbol{x},\omega)/\partial\boldsymbol{n}(\boldsymbol{x})$ are

$$\Phi_\mathrm{I}(\boldsymbol{x},\omega) = \int_\Gamma\int_\tau P[\boldsymbol{y}(\tau),\tau]\frac{\partial G[\boldsymbol{x},\boldsymbol{y}(\tau),\omega]}{\partial\boldsymbol{n}[\boldsymbol{y}(\tau)]}\,\mathrm{e}^{\mathrm{i}\omega\tau}\,\mathrm{d}\tau\,\mathrm{d}\Gamma \tag{4}$$

$$\frac{\partial\Phi_\mathrm{I}(\boldsymbol{x},\omega)}{\partial\boldsymbol{n}(\boldsymbol{x})} = \int_\Gamma\int_\tau P[\boldsymbol{y}(\tau),\tau]\frac{\partial^2 G[\boldsymbol{x},\boldsymbol{y}(\tau),\omega]}{\partial\boldsymbol{n}(\boldsymbol{x})\partial\boldsymbol{n}[\boldsymbol{y}(\tau)]}\,\mathrm{e}^{\mathrm{i}\omega\tau}\,\mathrm{d}\tau\,\mathrm{d}\Gamma \tag{5}$$

where $\boldsymbol{y}(\tau)$ is the moving source position at time τ, Γ is the source surface, $\boldsymbol{n}[\boldsymbol{y}(\tau)]$ is the UNV of the source surface, and $P[\boldsymbol{y}(\tau),\tau]$ is the static pressure on the source surface. The Green function in 2D free field is

$$G(\boldsymbol{x},\boldsymbol{y},\omega) = \frac{i}{4}H_0^{(1)}[kr(\tau)] \tag{6}$$

where $H_m^{(n)}$ is the Hankel function of the mth kind and nth order, k is the wavenumber, and the distance between the source and observer is

$$r(\tau) = |\boldsymbol{x} - \boldsymbol{y}(\tau)| \tag{7}$$

The numerical implementation of equations (4) and (5) is carried out using the Gauss–Legendre quadrature [**26**] combining with the fast Fourier transform.

3.2 Thin-body boundary element method

Consider the scattering of sound waves by the volute, and assume the volute is acoustically rigid. The total acoustic pressure is obtained as the sum of incident and scattered acoustic pressure

$$\Phi(\boldsymbol{x},\omega) = \Phi_\mathrm{I}(\boldsymbol{x},\omega) + \int_S \frac{\partial G(\boldsymbol{x},\boldsymbol{y},\omega)}{\partial\boldsymbol{n}(\boldsymbol{y})} \times [\Phi^+(\boldsymbol{y},\omega) - \Phi^-(\boldsymbol{y},\omega)]\,\mathrm{d}S(\boldsymbol{y}), \quad \boldsymbol{x}\notin S \tag{8}$$

When the observer locates on the smooth surface of the volute S, the following is obtained

$$\frac{1}{2}[\Phi^+(\boldsymbol{x},\omega) + \Phi^-(\boldsymbol{x},\omega)] = \Phi_\mathrm{I}(\boldsymbol{x},\omega) + \int_S \frac{\partial G(\boldsymbol{x},\boldsymbol{y},\omega)}{\partial\boldsymbol{n}(\boldsymbol{y})} \times [\Phi^+(\boldsymbol{y},\omega) - \Phi^-(\boldsymbol{y},\omega)]\,\mathrm{d}S(\boldsymbol{y}), \quad \boldsymbol{x}\in S \tag{9}$$

where $\Phi^+(\boldsymbol{y},\omega)$ and $\Phi^-(\boldsymbol{y},\omega)$ are the acoustic pressure on the inner and outer surfaces, respectively. Equation (9) is not sufficient to define the boundary integral representation for the two unknowns $\Phi^+(\boldsymbol{x},\omega)$ and $\Phi^-(\boldsymbol{x},\omega)$. Differentiating equation (9) with respect

to the UNV $\boldsymbol{n}(\boldsymbol{x})$ yields

$$0 = \frac{\partial \Phi_{\mathrm{I}}(\boldsymbol{x},\omega)}{\partial \boldsymbol{n}(\boldsymbol{x})} - \int_S \frac{\partial^2 G(\boldsymbol{x},\boldsymbol{y},\omega)}{\partial \boldsymbol{n}(\boldsymbol{y})\partial \boldsymbol{n}(\boldsymbol{x})} \times [\Phi^+(\boldsymbol{y},\omega) - \Phi^-(\boldsymbol{y},\omega)]\,\mathrm{d}S(\boldsymbol{y}), \quad \boldsymbol{x} \in S \tag{10}$$

where $\Phi_{\mathrm{I}}(\boldsymbol{x},\omega)$ and $\partial\Phi_{\mathrm{I}}(\boldsymbol{x},\omega)/\partial\boldsymbol{n}(\boldsymbol{x})$ are computed from equations (4) and (5), and

$$\frac{\partial G(\boldsymbol{x},\boldsymbol{y},\omega)}{\partial \boldsymbol{n}[\boldsymbol{y}(\tau)]} = \frac{\mathrm{i}k}{4}\frac{H_1^{(1)}[kr(\tau)]}{r(\tau)}[\boldsymbol{x}-\boldsymbol{y}(\tau)]\,\boldsymbol{n}[\boldsymbol{y}(\tau)] \tag{11}$$

$$\frac{\partial^2 G(\boldsymbol{x},\boldsymbol{y},\omega)}{\partial \boldsymbol{n}(\boldsymbol{x})\partial \boldsymbol{n}[\boldsymbol{y}(\tau)]} = \left\{\frac{ik^2 H_0^{(1)}[kr(\tau)]}{4} - \frac{\mathrm{i}kH_1^{(1)}[kr(\tau)]}{2r(\tau)}\right\} \times \frac{\boldsymbol{r}\,\boldsymbol{n}(\boldsymbol{x})}{r}\frac{\boldsymbol{r}\,\boldsymbol{n}(\boldsymbol{y}(\tau))}{r} + \frac{\mathrm{i}k}{4r(\tau)}H_1^{(1)}[kr(\tau)]\,\boldsymbol{n}(\boldsymbol{x})\,\boldsymbol{n}[\boldsymbol{y}(\tau)] \tag{12}$$

The integral equations (8) to (10) are solved numerically using the isoparametric BEM. The numerical formulae of equations (9) and (10) can be written in matrix form as

$$\begin{bmatrix} \frac{1}{2}\delta_{mn} - H_{mn} & \frac{1}{2}\delta_{mn} + H_{mn} \\ -K_{mn} & K_{mn} \end{bmatrix} \begin{Bmatrix} \Phi^+ \\ \Phi^- \end{Bmatrix} = \begin{Bmatrix} \Phi_I(\boldsymbol{x}_m,\omega) \\ \dfrac{\partial \Phi_I(\boldsymbol{x}_m,\omega)}{\partial \boldsymbol{n}(\boldsymbol{x}_m)} \end{Bmatrix} \tag{13}$$

where δ_{mn} is the Dirac function and

$$\mathrm{H}_{mn} = \frac{\mathrm{i}kS_n}{8}\int_{-1}^{1} \cos\alpha H_1^{(1)}(kr)\,\mathrm{d}\xi \tag{14}$$

$$K_{mn} = \frac{\mathrm{i}kS_n}{8}\int_{-1}^{1}\left\{\cos\alpha\cos\delta\left[kH_0^{(1)}(kr) - \frac{2H_1^{(1)}(kr)}{r}\right] - \cos\beta\frac{H_1^{(1)}(kr)}{r}\right\}\mathrm{d}\xi \tag{15}$$

$$\cos\alpha = \frac{\boldsymbol{r}\,\boldsymbol{n}(\boldsymbol{y})}{r} \tag{16}$$

$$\cos\delta = \frac{\boldsymbol{r}\,\boldsymbol{n}(\boldsymbol{x})}{r} \tag{17}$$

$$\cos\beta = \boldsymbol{n}(\boldsymbol{x})\,\boldsymbol{n}(\boldsymbol{y}) \tag{18}$$

S_n is the length of the nth discrete element on the wall of the volute. For equations (14) and (15), singular integrals appear when the source and observer belong to the same element, and the integrals can be evaluated as follows [**27**]

$$H_{mm} = 0 \tag{19}$$

$$K_{mm} = -\frac{\mathrm{i}k}{2}H_1^{(1)}\left(\frac{kS_m}{2}\right) + \frac{\mathrm{i}k^2}{4}\left[H_0^{(1)}\left(\frac{1}{2}kS_m\right)S_m + \frac{kS_m^2}{4}\int_{-1}^{1}H_1^{(1)}\left(\frac{1}{2}kS_m|\xi|\right)|\xi|\,\mathrm{d}\xi\right] \tag{20}$$

Equation (20) can be numerically solved using the Gauss–Legendre quadrature. When the source and observer do not belong to the same element, the regular integrals of equations (14) and (15) are also solved using the Gauss–Legendre quadrature.

3.3 Numerical validation

In order to validate the developed computational code, we consider an acoustically rigid flat plate of width $2d$ as shown in Fig. 3. The boundary coordinates of the plate are

$$-d \leqslant x \leqslant d, \quad y = 0 \tag{21}$$

The incident plane wave travels in the direction of the negative y-axis, and the sound pressure is given by

$$\Phi_{\mathrm{I}}(\boldsymbol{x},\omega) = \mathrm{e}^{-\mathrm{i}ky} \tag{22}$$

And the exact solution of the total acoustic pressure on the flat plate is [**28**]

$$\Phi(\boldsymbol{x},\omega) = (8\pi)^{1/2}\sum_{n=0}^{\infty}(-1)^n \times \left[\mathrm{i}\frac{Se_{2n}(\upsilon,0)Se_{2n}(\upsilon,\eta)}{N_{2n}^{(e)}(\partial/\partial u)Re_{2n}^{(3)}(\upsilon,\cosh u)|_{u=0}} + \frac{So_{2n+1}(\upsilon,0)So_{2n+1}(\upsilon,\eta)}{N_{2n+1}^{(o)}(\partial/\partial u)Ro_{2n+1}^{(3)}(\upsilon,\cosh u)|_{u=0}}\right] \tag{23}$$

where

$$\upsilon = kd, \quad \eta = \cos\upsilon, \quad 0 \leqslant \upsilon < 2\pi \tag{24}$$

Se and *So* are the Mathieu even and odd angular functions, respectively, $Re^{(3)}$ and $Ro^{(3)}$ are the Mathieu even and odd radial functions of the third kind, respectively, and $N_i^{(\mathrm{e})}$ and $N_i^{(\mathrm{o})}$ are defined by the following orthogonal relations

$$\int_0^{2\pi} Se_m(\upsilon,\cos\upsilon)Se_n(\upsilon,\cos\upsilon)\,\mathrm{d}\upsilon = \begin{cases} 0 & m \neq n \\ N_m^{(e)} & m = n \end{cases} \tag{25}$$

$$\int_0^{2\pi} So_m(\upsilon,\cos\upsilon)So_n(\upsilon,\cos\upsilon)\,\mathrm{d}\upsilon = \begin{cases} 0 & m \neq n \\ N_m^{(\mathrm{o})} & m = n \end{cases} \tag{26}$$

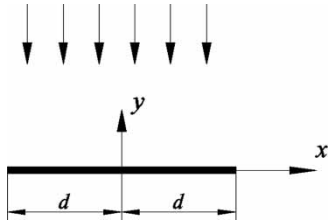

Fig. 3 Plane wave scattered by a rigid flat plate

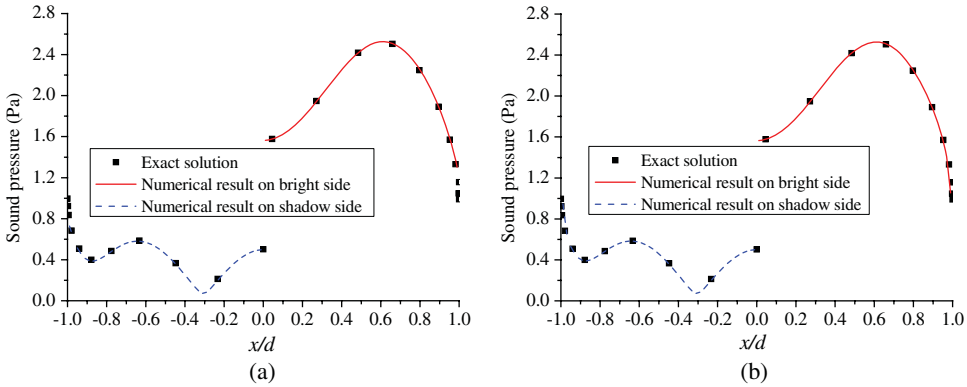

Fig. 4 Comparison of the sound pressure on the plate between the numerical result and the exact solution: (a) not using QPT and (b) using QPT

$$\int_0^{2\pi} Se_m(\upsilon, \cos\upsilon) So_n(\upsilon, \cos\upsilon)\, \mathrm{d}\upsilon = 0 \tag{27}$$

The flat plate is discretized with 100 isoparametric boundary elements, and Fig. 4(a) shows the numerical result and exact solution for the case of $k = 5$ and $d = 1$ m. At the most positions on the plate, a good agreement between numerical result and exact solution has been obtained, but the discrepancy appears at the edges of the plate, due to the effect of knife-edge diffraction [**29**]. In order to capture this phenomenon, the quarter point technique (QPT) proposed by Wu and Wan [**14**] is adopted, and Fig. 4(b) shows that there is much less computational error at the edge of the plate using QPT.

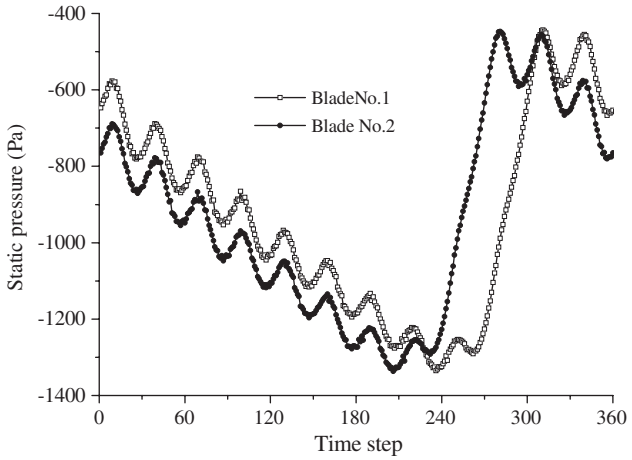

Fig. 5 Time histories of the pressure fluctuation on the neighbouring blades

4 RESULTS AND DISCUSSION

Figure 5 plots the time histories of the pressure fluctuation for two points during one impeller revolution, where the points locate on the neighbouring rotating blades and have the same radial coordinates. Because both the time histories nearly have the same shapes with a phase difference, we can deduce that the assumption in section 2 is reasonable.

In the present article, we just focus on the tonal noise of the centrifugal fan. And the blade passing frequency (BPF) of the centrifugal fan is

$$\mathrm{BPF} = \frac{nZ}{60} = 290\,\mathrm{Hz} \tag{28}$$

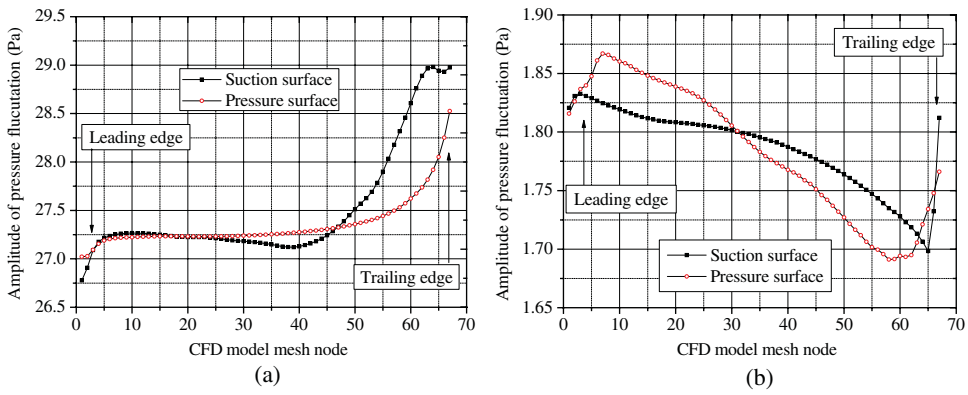

Fig. 6 Amplitude of pressure fluctuation on pressure surface and suction surface: (a) BPF and (b) 2BPF

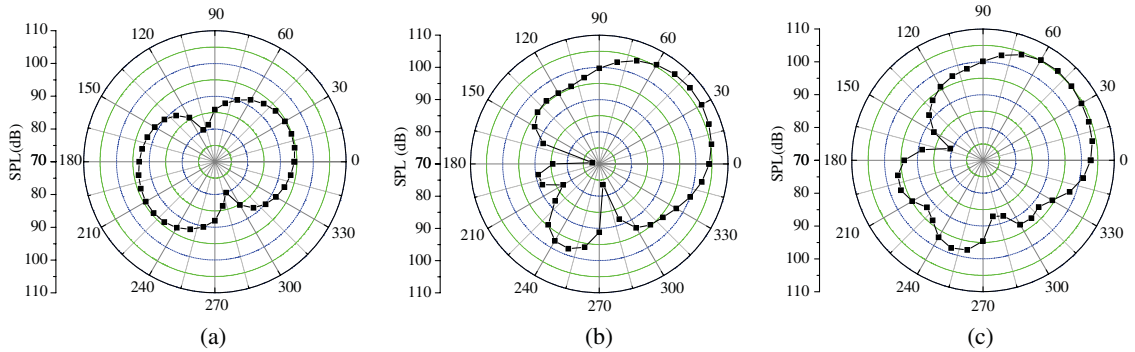

Fig. 7 Noise directivity pattern at the BPF: (a) free field; (b) scattering field; and (c) total field

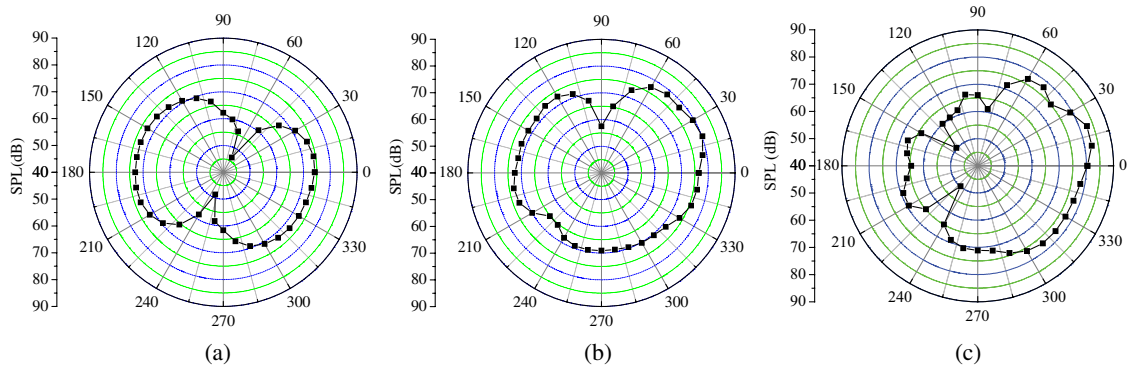

Fig. 8 Noise directivity pattern at the 2BPF: (a) free field; (b) scattering field; and (c) total field

where n is the rotational speed of the blades. Figure 6 shows the amplitudes of pressure fluctuation on the blade surface at the BPF and 2BPF. The amplitude of the pressure fluctuations at the BPF is much stronger than that at the 2BPF. Seen from Fig. 6(a), the pressure fluctuation near the leading edge nearly has the same amplitude, but an evident pressure difference exists in the vicinity of the trailing edge; hence the noise of the blades is mainly contributed from the sources in the vicinity of the trailing edge.

Acoustic pressure in frequency domain is computed by combing the FW–H equation and the thin-body BEM, and the sound pressure level (SPL) at the observer (R, θ), as shown in Fig. 1, is given by

$$\mathrm{SPL} = 20 \log_{10} \left[\frac{\Phi(\boldsymbol{x}, \omega)}{p_{\mathrm{ref}}} \right] \tag{29}$$

where p_{ref} $(= 2 \times 10^{-5}\,\mathrm{Pa})$ is the reference pressure.

For the case of $R = 3\,\mathrm{m}$, the noise directivity patterns at the BPF and 2BPF are shown in Figs 7 and 8, respectively. From these figures, we can see that the directivity patterns of the blades noise in free field give the well-known figure of eight-shaped feature, but the scattering of the volute not only changes the direction of noise propagation, but also enhances the SPL at the outlet of the volute. The same conclusion has been drawn from the experimental result of Moreland [**11**].

A detailed experimental study on this centrifugal fan has also been carried out [**30**]. The numerical SPLs at 1 m apart from the outlet of the volute are compared with the experimental data with regard to the BPF and its second harmonic component as shown in Fig. 9. Measurements are the combination of the following five aspects:

(a) noise of the blades scattered by the centrifugal volute;
(b) volute noise scattered by the non-compact centrifugal volute;
(c) volute noise scattered by the blades;

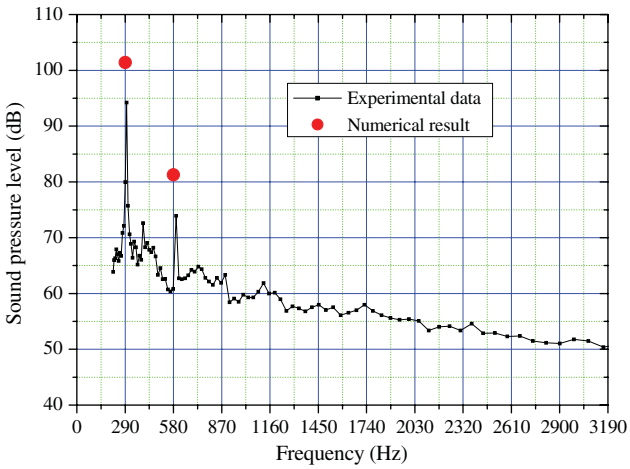

Fig. 9 Comparison of numerical and experimental SPLs

(d) noise of blades scattered by the non-compact blades;
(e) noise radiating from the driven motor.

The present article is focused on the first one, so comparisons of numerical and experimental data are not determinant.

5 CONCLUSIONS

This article presents a numerical method for predicting the rotating blades noise scattered by the volute. To obtain the aerodynamic noise source on the blades, the unsteady viscous flow in the centrifugal fan is simulated, and the FW–H equation and thin-body BEM are used to predict the noise of the blades scattered by the volute wall.

The numerical result has shown that the scattering of the volute not only changes the direction of noise propagation, but also enhances the SPL at the outlet of the volute. The developed numerical code has been validated by comparison of the numerical result and the exact solution of a simple scattering problem.

It should be noted that the present work has predicted the noise of the blades scattered by the centrifugal volute, but ignored the scattering effect of rotating blades. Hence, the computation of the noise of the fan scattered by the rotating blades should be carried out in the next work.

ACKNOWLEDGEMENT

The authors thank the anonymous reviewers for insightful comments and suggestions to improve the article.

REFERENCES

1 **Lu, H. Z., Huang, L. X., So, R. M C.,** and **Wang, J.** A computational study of the interaction noise from a small axial-flow fan. *J. Acoust. Soc. Am.*, 2007, **122**(3), 1404–1415.
2 **Maaloum, A., Kouidri, S.,** and **Rey, R.** Aeroacoustic performance evaluation of axial flow fans based on the unsteady pressure field on the blade surface. *Appl. Acoust.*, 2004, **65**, 367–384.
3 **Cho, Y.** and **Moon, Y. J.** Discrete noise prediction of variable pitch cross flow fans by unsteady Navier–Stokes computations. *ASME J. Fluids Eng.*, 2003, **125**, 543–550.
4 **Moon, Y. J., Cho, Y.,** and **Nam, H. S.** Computation of unsteady flow and aeroacoustic noise cross flow fans. *Comput. Fluids*, 2003, **32**, 995–1015.
5 **Suaráz, S. V., Tajadura, R. B., Morros, C. S.,** and **Francos, J. F.** Numerical prediction of the aerodynamic tonal noise in a centrifugal fan. In Proceedings of the ASME Fluids Engineering Division Summer Meeting, Montreal, Canada, July 2002, pp.1–8.
6 **Tajadura, R. B., Suaráz, S. V.,** and **Cruz, J. P. H.** Noise prediction of a centrifugal fan: numerical results and experimental validation. *ASME J. Fluids Eng.*, 2008, **130**, 091102-1–091102-12.
7 **Liu, Q., Qi, D.,** and **Mao, Y.** Numerical simulation of centrifugal fan noise. *Proc. IMechE, Part C: J. Mechanical Engineering Science*, 2006, **220**(C8), 1167–1178. DOI: 10.1243/09544062JMES211.
8 **Liu,Q., Qi, D.,** and **Tang, H.** Computation of aerodynamic noise of centrifugal fan using large eddy simulation approach, acoustic analogy, and vortex sound theory. *Proc. IMechE, Part C: J. Mechanical Engineering Science*, 2007, **221**(C11), 1321–1332. DOI: 10.1243/09544062JMES609.
9 **Younsi, M., Bakir F., Kouidri, S.,** and **Rey, R.** Numerical study and experimental study of unsteady flow in a centrifugal fan. *Proc. IMechE, Part A: J. Power and Energy*, 2007, **221**(A7), 1025–1036. DOI: 10.1243/09576509JPE445.
10 **Khelladi, S. V., Bakir. F.,** and **Rey, R.** Predicting tonal noise from a high rotational speed centrifugal fan. *J. Sound Vibr.*, 2008, **313**, 113–133.
11 **Moreland, J. B.** Housing effects on centrifugal blower noise. *J. Sound Vibr.*, 1974, **36**, 191–205.
12 **Langthjem, M. A.** and **Olhoff, N.** A numerical study of flow-induced noise in a two-centrifugal pump. Part II. Hydroacoustics. *J. Fluid Struct.*, 2004, **19**, 369–386.
13 **Martinez, R.** The thin-shape breakdown of the Helmholtz integral equation. *J. Acoust. Soc. Am.*, 1991, **90**, 2728–2738.
14 **Wu, T. W.** and **Wan, G. C.** Numerical modeling of acoustic radiation and scattering from thin bodies using a Cauchy principal integral equation. *J. Acoust. Soc. Am.*, 1992, **92**, 2900–2906.
15 **Wu, T. W.** A direct mixed-boundary element method for mufflers with internal thin components covered by thin and a perforated panel. *J. Comput. Acoust.*, 2007, **15**, 145–157.
16 **Premat, E.** and **Gabillet, Y.** A new boundary-element method for predicting outdoor sound propagation and application to the case of a sound barrier in the presence of downward refraction. *J. Acoust. Soc. Am.*, 2000, **108**, 2775–2783.
17 **Cho, H. L.** and **Lee, D. J.** Development of the numerical method for calculating sound radiation from a rotating dipole source in an opened thin duct. *J. Sound Vibr.*, 2006, **295**, 739–752.
18 **Mao, Y., Qi, D., Liu, X.,** and **Tang, H.** Numerical prediction of aerodynamic tonal noise radiated from a centrifugal fan. *Proc. IMechE, Part A: J. Power and Energy*, 2008, **222**(A8), 831–842. DOI: 10.1243/09576509JPE655.
19 **Qi, D. T., Pomfret, M. J.,** and **Lam, K.** A new approach to the design of fan volute profiles. *Proc. IMechE, Part C: J. Mechanical Engineering Science*, 1996, **210**(C3), 287–294. DOI: 10.1243/PIME_PROC_1996_210_198_02.
20 **Zhang, K. W.** *Principle of fluid machinery*, 2001 (China Machine Press, Beijing).
21 **Ffowcs Williams, J. E.** and **Hawkings, D. L.** Sound generation by turbulence and surfaces in arbitrary motion. *Philos. Trans. R. Soc.*, 1969, **A264**, 321–342.

22 Neise, W. Noise reduction in centrifugal fans: a literature survey. *J. Sound Vibr.*, 1976, **45**, 375–403.

23 Nesie, W. Review of fan noise generation mechanisms and control methods. In Proceedings of the Second International INCE Symposium, Senlis, France, 1992, pp. 45–56.

24 Lockard, D. P. An efficient two-dimensional implementation of the Ffowcs Williams and Hawkings equation. *J. Sound Vibr.*, 2000, **229**, 897–911.

25 Guo, Y. P. Application of the Ffowcs William/Hawkings equation to two-dimensional problems. *J. Fluids Mech.*, 2000, **403**, 201–221.

26 Ma, Z. H. *Handbook of applied mathematics*, 2005 (Tsinghua University Press, Beijing).

27 Chen, K. H. and **Chen, J. T.** Dual boundary element analysis of oblique incident wave passing a thin submerged breakwater. *Eng. Anal. Bound. Elem.*, 2002, **26**, 917–927.

28 Bowman, J. J., Senior, T. B. A., and **Uslenghi P. L. E.** *Electromagnetic and acoustic scattering by simple shapes*, 1969 (North-Holland Publishing Company, Amsterdam).

29 Morse, P. M. and **Ingrad, K. U.** *Theoretical acoustics*, 1968 (McGraw-Hill Company, New York).

30 Mao, Y., Qi, D., Liu, X., and **Yuan, M.** Experimental study on the noise reduction of an industrial forward-curved blades centrifugal fan. *Appl. Acoust.*, 2009, **70**, 1041–1050.